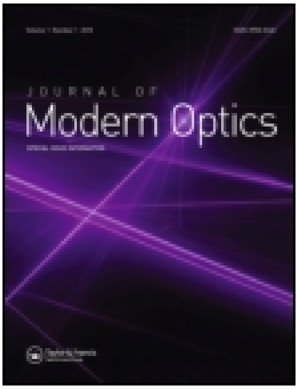

Journal of Modern Optics
Publication details, including instructions for authors and subscription information:
http://www.tandfonline.com/loi/tmop20

Analytical and Numerical Approximations in Fresnel Diffraction

E. Carcolé [a], S. Bosch [a] & J. Campos [a]

[a] Department de Física Applicada i Electrònica, Universitat de Barcelona, Diagonal 647, 08028, Barcelona, Spain

Available online: 01 Mar 2007

To cite this article: E. Carcolé, S. Bosch & J. Campos (1993): Analytical and Numerical Approximations in Fresnel Diffraction, Journal of Modern Optics, 40:6, 1091-1106

To link to this article: http://dx.doi.org/10.1080/09500349314551161

JOURNAL OF MODERN OPTICS, 1993, VOL. 40, NO. 6, 1091–1106

Analytical and numerical approximations in Fresnel diffraction

Procedures based on the geometry of the Cornu spiral

E. CARCOLÉ, S. BOSCH and J. CAMPOS

Universitat de Barcelona, Departament de Física Applicada i Electrònica, Diagonal 647, 08028 Barcelona, Spain

(*Received 7 October 1992; revision received 6 January 1993*)

Abstract. Procedures for the fast and accurate numerical computation of Fresnel diffraction integrals are developed on the basis of geometrical properties of the Cornu spiral. The methods proposed allow the highly oscillatory integrals in Fresnel diffraction to be approximated by means of three simpler integrals and permit the calculation of these final integrals using analytical formulae.

1. Introduction

Fraunhofer and Fresnel diffraction are classical topics in wave optics. Most practical problems may be satisfactorily treated within the well known Fraunhofer approximation but, in many cases, the more general Fresnel treatment is necessary. In many cases, the more general Fresnel treatment is necessary. In the calculation of Fraunhofer diffraction patterns the fast Fourier transform algorithm may be used, as the figures correspond to Fourier transforms of the diffracting object. For Fresnel diffraction, the problem leads to the computation of a different integral for each point of the pattern. These integrals may be difficult (time consuming) to evaluate when the integrand is highly oscillatory within the integration zone. Therefore, several numerical techniques have been used for computations [1], together with approximate procedures requiring short calculation times [2, 3].

Assuming that the conditions for the validity of Fresnel diffraction are fulfilled, there are two important practical reasons for studying the diffraction of a rectangle as a tool to solve two-dimension problems. First, the two-dimensional integration problem may be reduced (by decomposition of the function defining the aperture into many rectangles) to many simple rectangular cases. Second, the interesting case of pixelated spatial light modulators [4], giving apertures of variable complex transmittance, may easily be dealt with by treating each pixel as a rectangle. For this important practical case, it is of primary importance to use fast computation procedures, as a diffraction problem has to be solved for each one of the pixels.

The aim of the present paper is to develop simple geometrical procedures for the computation of Fresnel-type integrals in the near field. The resulting accuracy is about 1% (or better) relative error in the computation of complex amplitudes and the calculation is 30 times faster than numerical integration. This accuracy is similar to the Fresnel approximation itself in the near field [2]. All the computation procedures apply to diffraction apertures and to obstructions by simple application of Babinet's principle.

0950-0340/93 $10·00

2. Diffraction geometry. The Cornu spiral

In our development, notations follow Klein and Furtak [5]. The general diffraction set-up is sketched in figure 1. The complex amplitude at a point $P'(x', y')$ of the final plane, when the diffraction aperture is a rectangle is given by

$$E'(P') = \frac{\mathrm{i}}{\pi} E'_{na}(P') \int_{\eta_{x_1}}^{\eta_{x_2}} \int_{\eta_{y_1}}^{\eta_{y_2}} \exp\left[-\mathrm{i}(x^2+y^2)\right] \mathrm{d}x\, \mathrm{d}y, \tag{1}$$

where

$$\eta_{x_1} = \frac{x'_1 - x'}{F}, \qquad \eta_{x_2} = \frac{x'_2 - x'}{F},$$

$$\eta_{y_1} = \frac{y'_1 - y'}{F}, \qquad \eta_{y_2} = \frac{y'_2 - y'}{F},$$

$$F = \left[\frac{\lambda D'(D+D')}{\pi D}\right]^{1/2}, \tag{2}$$

and $E'_{na}(P')$ is the field without any aperture. Note that the exponential and the definition of F have been slightly modified from the definitions given in [5] in order to obtain simpler final integrals. This implies a parametrization in η that is different from the more customary form, and that includes a $\pi/2$ factor in the exponential.

Following our definitions, it is important to note that $\Delta\eta = \eta_2 - \eta_1$ (both for x and y) is constant for any calculation point (x', y') on a fixed plane.

Thus, calculating complex amplitudes in Fresnel diffraction is equivalent to computing integrals of the type

$$\int_0^{\eta} \exp(-\mathrm{i}x^2)\, \mathrm{d}x, \tag{3}$$

known as the complex Fresnel integrals. These integrals are not analytically resolvable and their numerical computation becomes time consuming because of

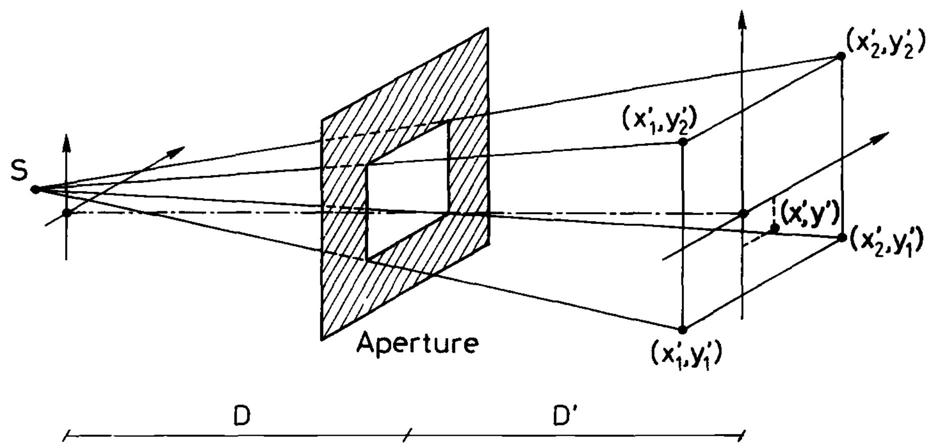

Figure 1. Geometrical configuration.

the highly oscillatory behaviour of the integrand. Plotting the real and imaginary parts of (3) on the complex plane as a function of the parameter η, the well known Cornu spiral is obtained (see figure 2).

A striking feature of this figure is the simple dependence of relevant geometrical properties on the value η. For example [6, 7]:

(i) the length s along the curve (from the origin) is given by

$$s=|\eta|, \tag{4}$$

(ii) the angle between the real axis and the tangent to the curve at a point defined by η is given by

$$\theta=-\eta^2, \tag{5}$$

(iii) the curvature radius at a point defined by η is

$$\rho=\left|\frac{1}{2\eta}\right|, \tag{6}$$

(iv) the value of the integral for the full η range is

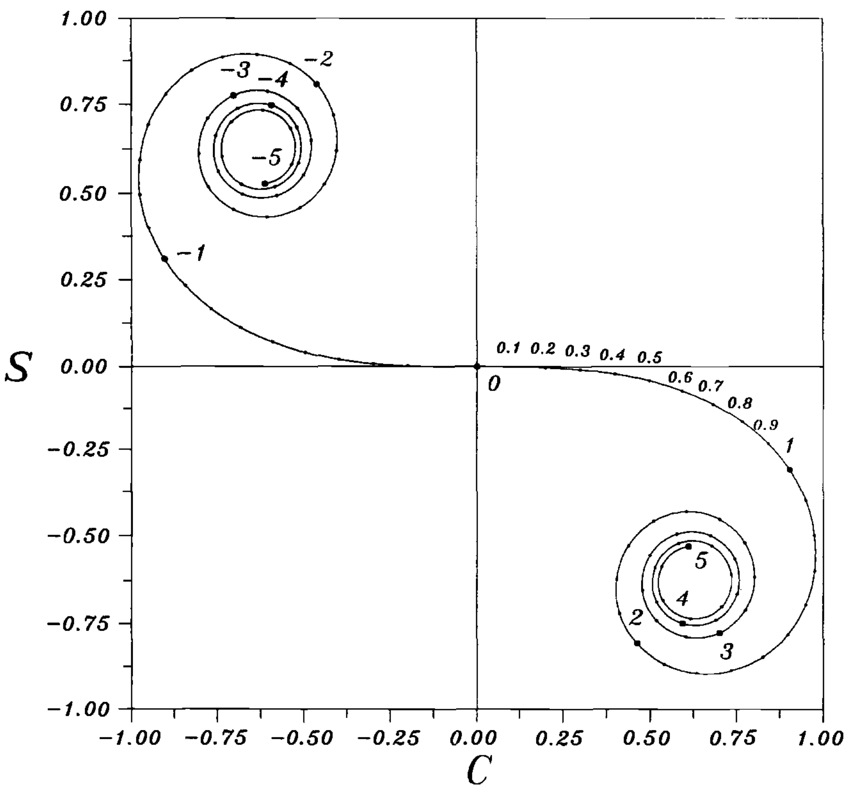

Figure 2. Plot of the real (C) and imaginary (S) parts of the Fresnel integrals as a function of the parameter η (Cornu spiral). Several values of η are indicated on the curve.

$$\int_0^{\infty} \exp(\mathrm{i}x^2)\,\mathrm{d}x=\frac{1}{2}\int_{-\infty}^{\infty} \exp(-\mathrm{i}x^2)\,\mathrm{d}x=\frac{1}{2}\left(\frac{\pi}{2}\right)^{1/2}(1-\mathrm{i}). \quad (7)$$

We will see that these four properties have an important role in the development of approximate mathematical expressions for the calculation of Fresnel integrals.

3. Geometrically based approximations for the Cornu spiral

Focusing our attention on property (iii) above, it is apparent that the curvature radius decreases rapidly as η increases. Moreover, this property also implies that the variation of the curvature radius will depend on $1/\eta^2$, i.e weakly dependent on η, as η increases. Thus, for large η and a limited range of variation in η, the curvature radius will be almost constant. This is the key point in the forthcoming developments and becomes our central assumption.

In order to use approximations derived from the previous properties, it is necessary to write the integral (3) in the form

$$\int_0^{\eta} \exp(-\mathrm{i}x^2)\,\mathrm{d}x=\int_0^{\infty} \exp(-\mathrm{i}x^2)\,\mathrm{d}x+\int_{\infty}^{\eta} \exp(-\mathrm{i}x^2)\,\mathrm{d}x=I_0^{\infty}+I_{\infty}^{\eta}, \quad (8)$$

(see figure 3), since I_{∞}^{η} will adequately be approximated by taking into account the factors just discussed.

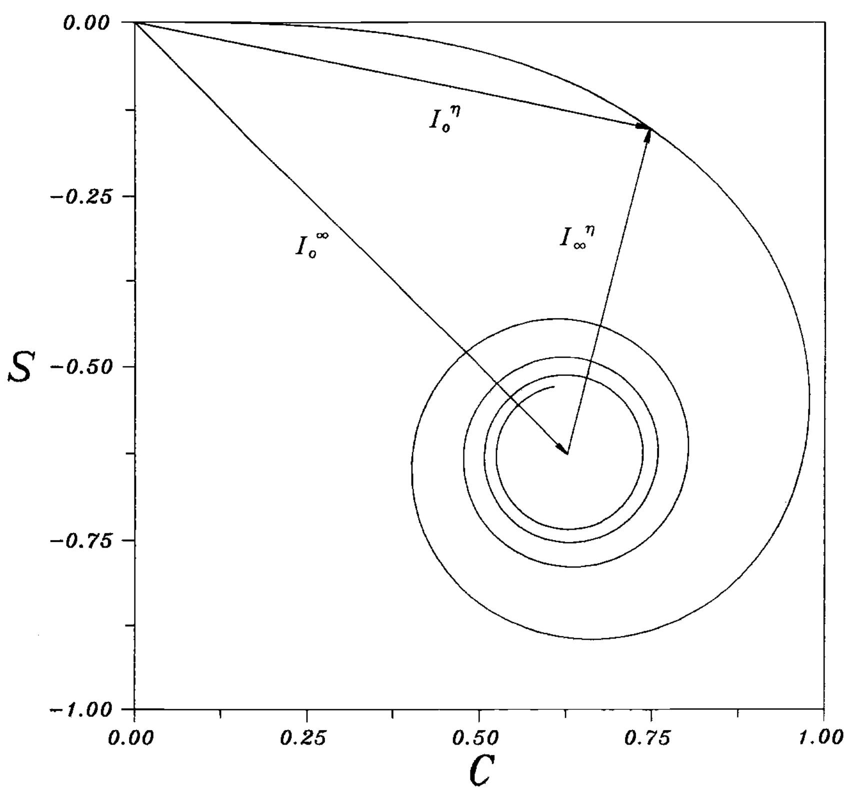

Figure 3. Illustrating I_0^{η} as a complex sum of I_0^{∞} and I_{η}^{∞}.

Let us begin by defining the integrals I_1, I_2, I_3 and I_4, whose graphical interpretation is illustrated in figure 4, an enlarged portion of the most coiled part of figure 3.

$$I_1=\int_{\eta}^{(\eta^2+\pi)^{1/2}} \exp(-\mathrm{i}x^2)\,\mathrm{d}x, \qquad I_2=\int_{(\eta^2+\pi)^{1/2}}^{(\eta^2+2\pi)^{1/2}} \exp(-\mathrm{i}x^2)\,\mathrm{d}x,$$

$$I_3=\int_{\eta}^{(\eta^2+2\pi)^{1/2}} \exp(-\mathrm{i}x^2)\,\mathrm{d}x, \qquad I_4=\int_{(\eta^2+2\pi)^{1/2}}^{(\eta^2+3\pi)^{1/2}} \exp(-\mathrm{i}x^2)\,\mathrm{d}x. \tag{9}$$

Note that, after property (ii) of Section 2, an increment of π in the square of the integration limit corresponds to the opposite side of the spiral (slope of opposite sign).

A first approximation may be proposed:

$$I_{\infty}^{\eta}\approx I_a\equiv -\frac{1}{2}I_1. \tag{10}$$

It is easy to see that this estimation has a lower modulus than the exact value.

Careful analysis of figure 4 suggests an initial refinement to the previous expression

$$I_{\infty}^{\eta}\simeq I_b\equiv -\left(I_1+\frac{1}{2}I_2\right). \tag{11}$$

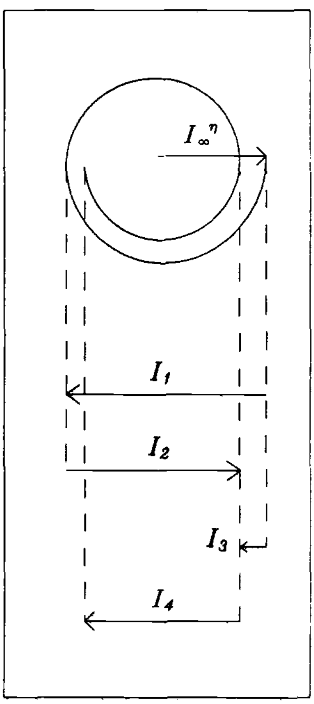

Figure 4. Sketch of the definition of the quantities I_1, I_2, I_3 and I_4.

It is easy to check that this is in fact a better approximation than I_a; this is due to using higher η values, a condition for the validity of our key point just mentioned in Section 2.

Actually, I_b gives values higher in modulus than the correct ones. A more accurate approximation is obtained by taking I_c as:

$$I_\infty^\eta \simeq I_c \equiv -\left(I_1 + I_2 + \frac{1}{2} I_4\right) = -\left(I_3 + \frac{1}{2} I_4\right). \tag{12}$$

This is indeed a better estimation, as it uses even higher η values; in fact I_c also gives a lower estimate, but better than I_a.

Note that we are only using the three integrals I_1, I_2, I_4 to develop the approximations. The formulae presented correspond to taking the first terms of a more general development:

$$\begin{aligned} I_\infty^\eta \simeq & \sum_{j=0}^{j=N-2} \int_{(\eta^2+\pi)^{1/2}}^{[\eta^2+(j+1)\pi]^{1/2}} \exp(-\mathrm{i}x^2)\,\mathrm{d}x \\ & + \frac{1}{2} \int_{[\eta^2+(N-1)\pi]^{1/2}}^{(\eta^2+N\pi)^{1/2}} \exp(-\mathrm{i}x^2)\,\mathrm{d}x, \quad N=2, 3 \ldots \\ = & \int_{\eta}^{[\eta^2+(N-1)\pi]^{1/2}} \exp(-\mathrm{i}x^2)\,\mathrm{d}x \\ & + \frac{1}{2} \int_{[\eta^2+(N-1)\pi]^{1/2}}^{(\eta^2+N\pi)^{1/2}} \exp(-\mathrm{i}x^2)\,\mathrm{d}x, \quad N=1, 2, 3 \ldots . \end{aligned} \tag{13}$$

Our interest is not to use more than three intervals for integration (provided the final precision is sufficient), so we will basically construct new approximations from I_b and I_c only.

The graphical representations of the accuracy of the preceding approximations (and also of those soon to be defined) are presented in figures 5 (*a*) and (*b*). Figure 5 (*a*) is a plot of the relative error in the modulus originated by the different approximations I_a, I_b, I_c as a function of the η value. The sign near the identification of the curves indicates the sign of the relative error, i.e. values greater than or less than exact values. Figure 5 (*b*) shows the absolute error in the calculation of the phase by the different definitions I_a, I_b, ... All the integrals were calculated using the Romberg method [8], to a fractional accuracy of 10^{-6}, with five points used for extrapolation. For I_∞^η to be computed without approximation, equality (8) was taken into account to avoid the infinitely oscillatory behaviour of the integrand, which would make the convergence of numerical integration more difficult.

Observing the characteristics of curves (*b*) and (*c*) in figure 5, it is evident that the following definition leads to a better approximation

$$I_\infty^\eta \simeq I_d \equiv \frac{1}{2} I_b + \frac{1}{2} I_c = -\left(I_1 + \frac{3}{4} I_2 + \frac{1}{4} I_4\right). \tag{14}$$

The corresponding accuracies are plotted in the same figures. Clearly, I_d represents a good fitting, mainly regarding its asymptotic behaviour. Furthermore, this suggests new definitions as

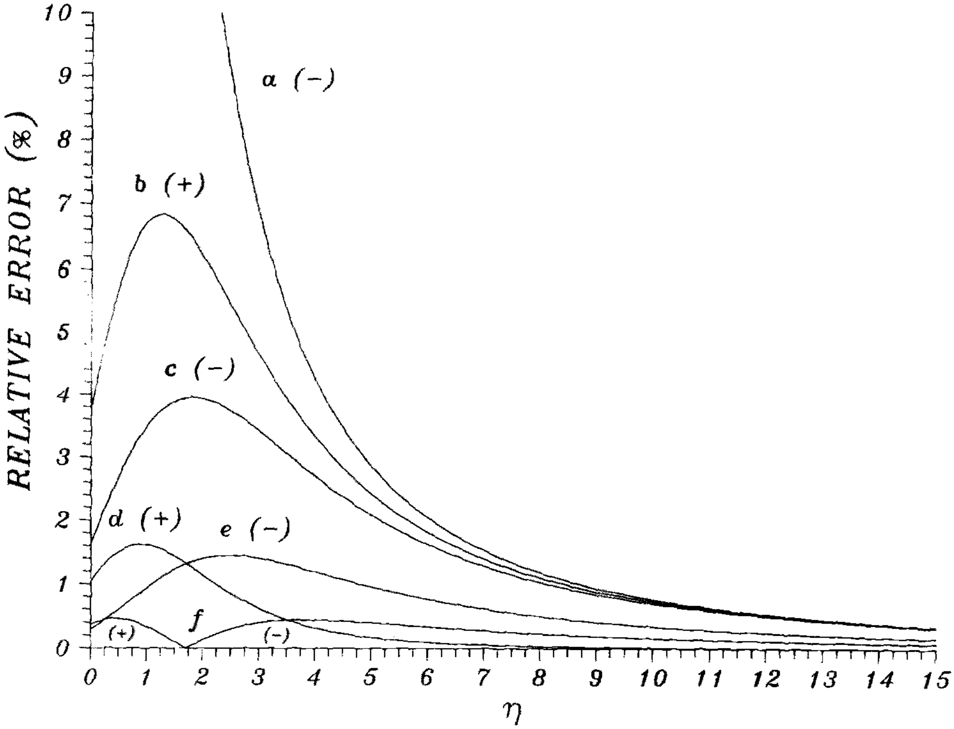

(a)

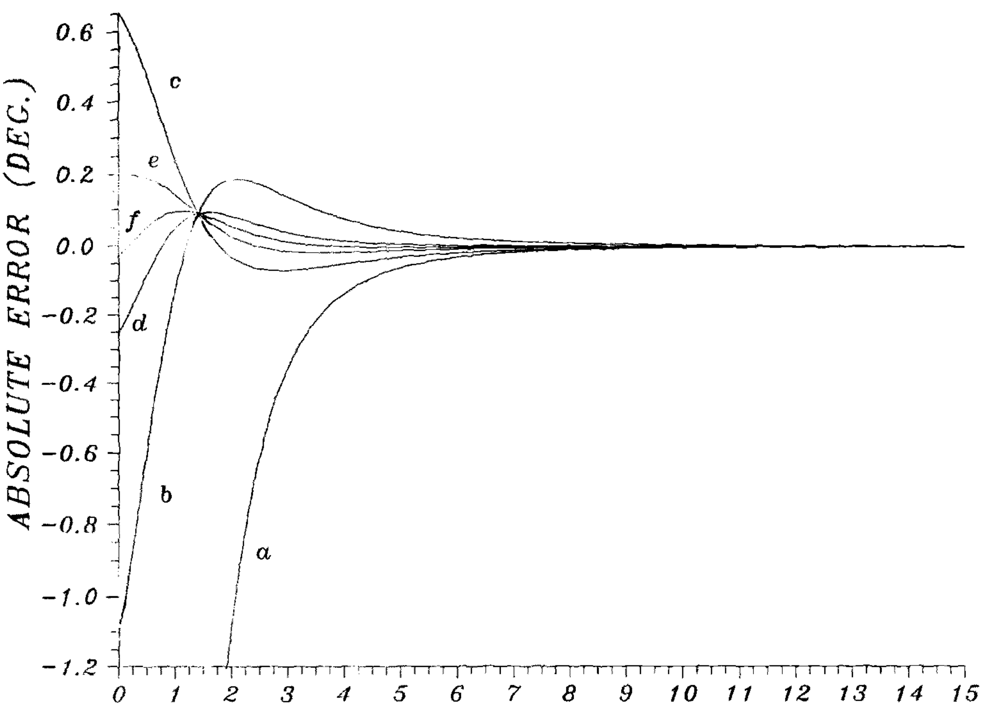

(b)

Figure 5. (*a*) Relative error in the modulus of I_∞^η when approximations $I_a, \ldots, I_f$ are used and $I_1, \ldots, I_4$ are numerically computed. (*b*) Absolute error in the phase of I_∞^η when approximations $I_a, \ldots, I_f$ are used and $I_1, \ldots, I_4$ are numerically computed.

$$I^{\eta}_{\infty} \simeq I_e \equiv \frac{1}{2}(I_c + I_d) = -\left(I_1 + \frac{7}{8} I_2 + \frac{3}{8} I_4\right), \tag{15}$$

whose behaviour is good for small η values, but worse for greater ones. From the analysis of the curves (*d*) and (*e*), their opposite sign and the fact that there is a crossing point lead to a final definition

$$I^{\eta}_{\infty} \simeq I_f \equiv \frac{1}{2}(I_d + I_e) = -\left(I_1 + \frac{13}{16} I_2 + \frac{5}{16} I_4\right). \tag{16}$$

As was our purpose, for all our definitions we use only three different Fresnel type integrals, as in (9), which always implies simple numerical integration.

In conclusion, examination of figure 5 suggests combining the use of $I_f(0<|\eta|<3{\cdot}5)$ and $I_d(|\eta|>3{\cdot}5)$, which results in a simple computation procedure whose relative error for the modulus is always better than 0·5% and similar for the phase. Indeed, when $0<|\eta|<3{\cdot}5$ direct evaluation of integrals is better (faster) than using the proposed decompositions, as they do not have a highly oscillatory integrand. In conclusion, the proposed method for computing I^{η}_{∞} is:

(*a*) for $\eta<3{\cdot}5$ numerical integration,
(*b*) for $\eta>3{\cdot}5$ use I_d.

We designate this the geometrically based numerical approximation (GNA).

More accurate results can be obtained by taking a higher N value in (13). As an even N value implies obtaining results higher than the correct ones and odd N values the opposite, a simple mean of them will always be a better estimation.

4. Simple geometrically-based analytical expressions for the integrals of interval π in the Cornu spiral

Our aim is to find simple but precise analytical expressions for integrals of the type

$$I_{\pi}(\eta) \equiv \int_{\eta}^{(\eta^2+\pi)^{1/2}} \exp(-\mathrm{i}x^2)\,\mathrm{d}x \equiv M \exp(\mathrm{i}\varphi) \tag{17}$$

with a view to avoiding numerical integrations if possible.

Let us begin with the modulus M. Inspecting figure 6, our basic assumption about the curvature radius of the Cornu spiral (after properties (iii) and (i) of Section 2), allows us to approximate the shape of the curve between η and $(\eta^2+\pi)^{1/2}$ to a circumferance of radius r, so it is easy to establish the equality

$$2l \simeq 2\pi r \equiv \pi M. \tag{18}$$

where l is the length along the spiral; therefore

$$l = (\eta^2+\pi)^{1/2} - \eta, \tag{19}$$

and, finally, from equations (18) and (19),

$$M \simeq \frac{2}{\pi}[(\eta^2+\pi)^{1/2} - \eta]. \tag{20}$$

Although it may seem a simple approximation, mainly for small η values, figure 7 (*a*) shows how accurately it describes the exact values of the integral.

The maximum relative error is 1·4% for $\eta=0$ and precision increases very rapidly with η.

The problem may be envisaged in a similar fashion for the phase φ of integral (17). For a true semi-circumference, the angle α in figure 6 would be exactly $\alpha=1/M=1/2r=\pi/2$. Our interest is to find a good approximation for α, using the previous approximation for M and a new expression for l. We see in figure 6 that

$$\varphi \simeq -\eta^2-\frac{l}{2r}. \tag{21}$$

From our previous modulus calculation, we may take r as

$$r=\frac{l}{\pi}=\frac{1}{\pi}[(\eta^2+\pi)^{1/2})-\eta]. \tag{22}$$

Similarly, along the integration interval we know that the curvature radius varies from $1/\eta$ to $1/(\eta^2+\pi)^{1/2}$. So, it becomes natural to take an intermediate value for r by using an adjusting parameter $k(0<k<1$, to be computed). Thus a new expression for l may be written as

$$l \simeq \pi \frac{1}{2(\eta^2+k\pi)^{1/2}}. \tag{23}$$

Finally φ is approximated as:

$$\varphi=-\eta^2-\left(\frac{\pi}{2}\right)^2\frac{1}{(\eta^2+k\pi)^{1/2}[(\eta^2+\pi)^{1/2}-\eta]}. \tag{24}$$

Other approximate formulae could be derived, for our simple expression leads to very accurate results even at low η values.

Equations (20) and (24) determine the quantities defined in (17). Figure 7(*b*) shows the absolute error in computations when the phase is estimated using the last

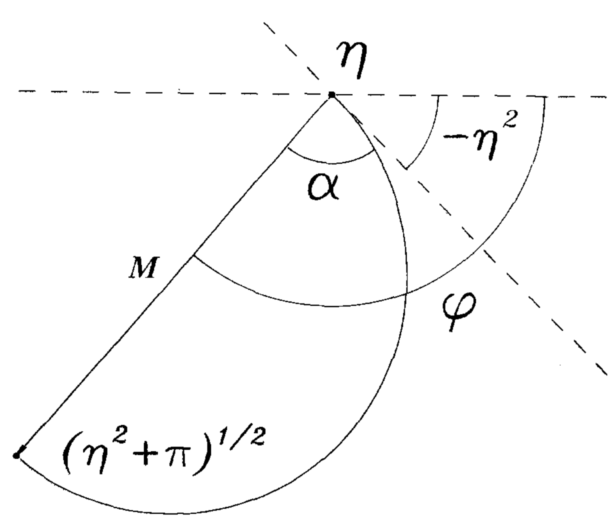

Figure 6. Illustrating the parameters used for computing M and φ approximately.

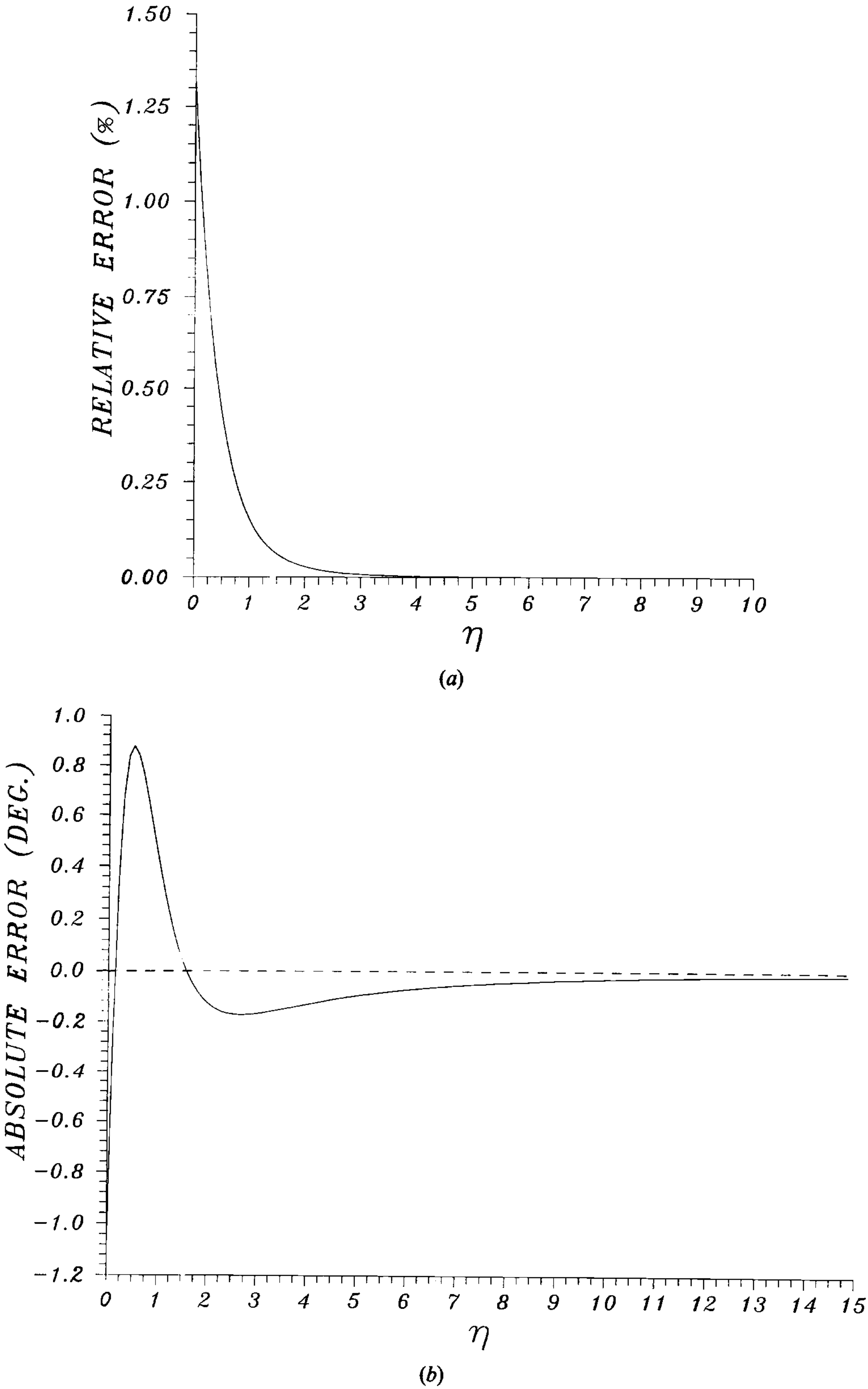

Figure 7. (*a*) Relative error in the modulus M when approximation (20) is used. (*b*) Absolute error in the phase φ when approximation (24) with $k=0{\cdot}68$ is used.

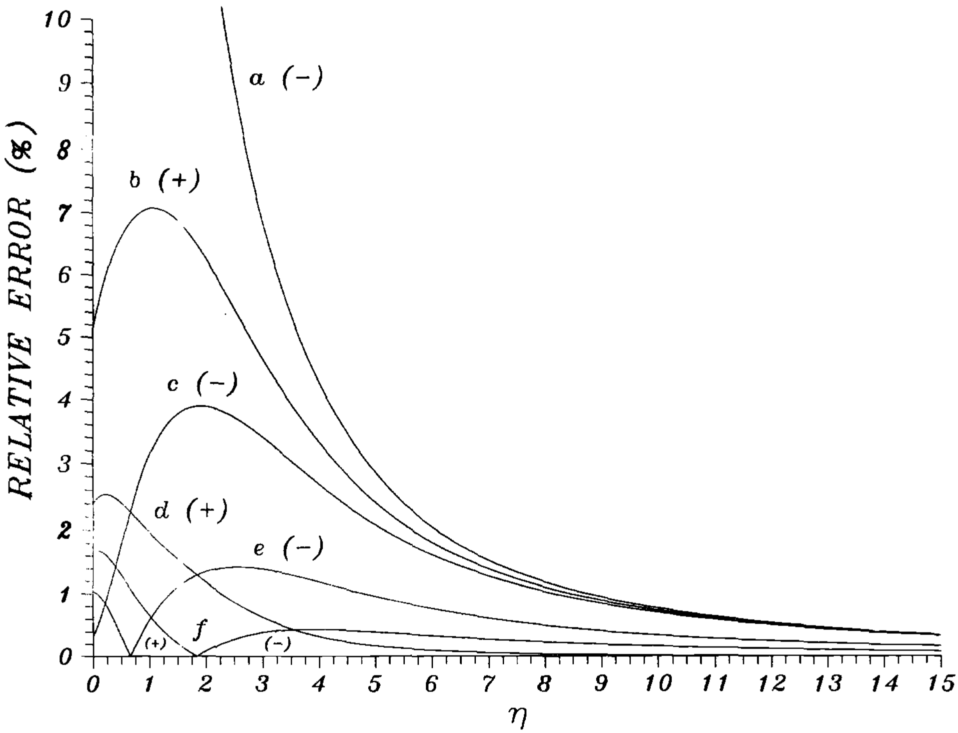

(*a*)

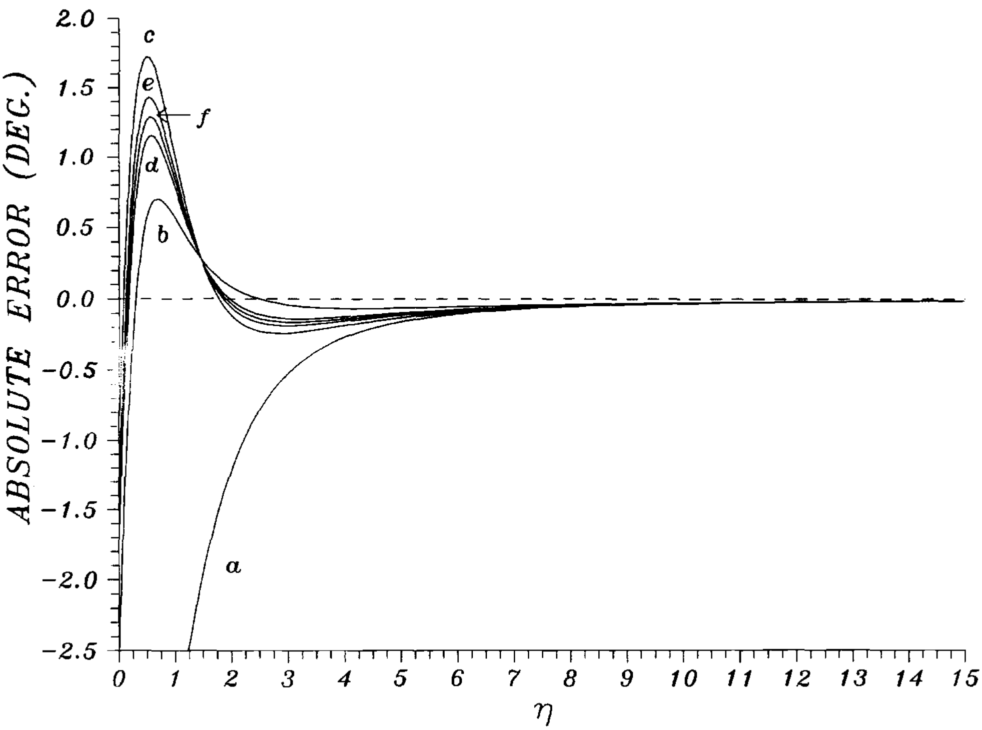

(*b*)

Figure 8. (*a*) Relative error in the modulus of I_∞^η when approximations $I_a, \ldots, I_f$ are used and $I_1, \ldots, I_4$ are are analytically estimated. (*b*) Absolute error in the phase of I_∞^η when approximations $I_a, \ldots, I_f$ are used and $I_1, \ldots, I_4$ are analytically estimated.

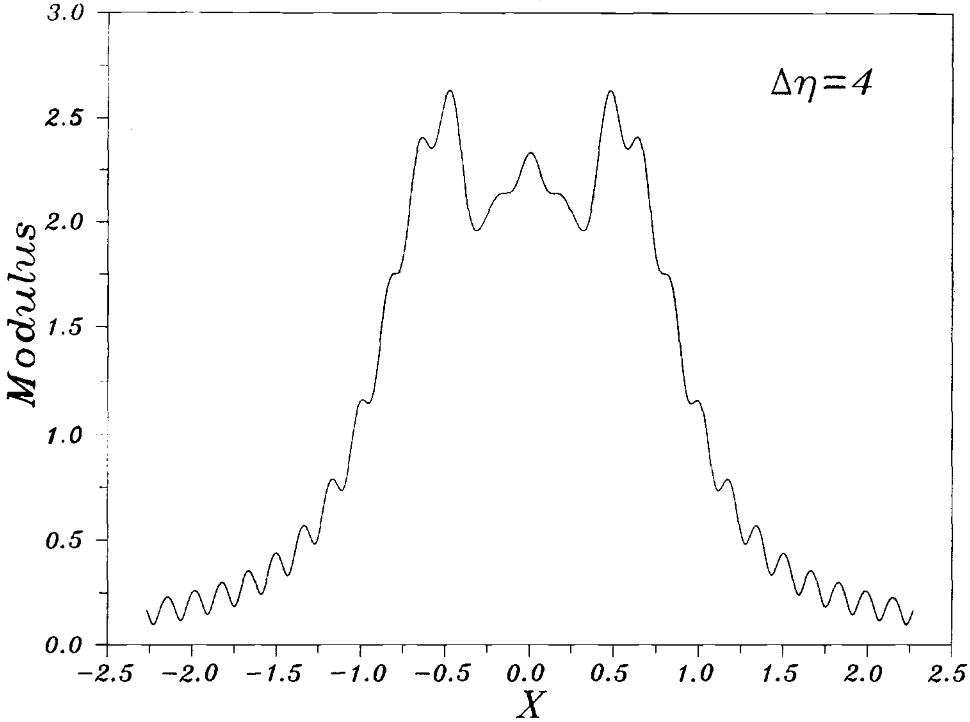

3.0
2.5
2.0
1.5
1.0
0.5
0.0
Modulus
Δη=4
−2.5 −2.0 −1.5 −1.0 −0.5 0.0 0.5 1.0 1.5 2.0 2.5
X

(*a*)

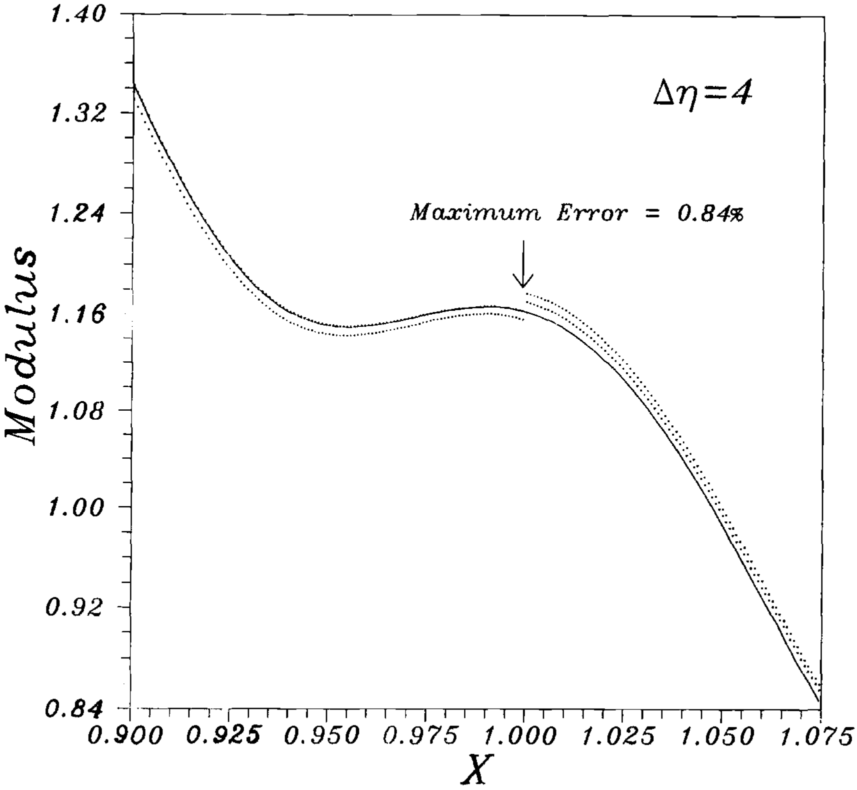

1.40
1.32
1.24
1.16
1.08
1.00
0.92
0.84
Modulus
Δη=4
Maximum Error = 0.84%
0.900 0.925 0.950 0.975 1.000 1.025 1.050 1.075
X

(*b*)

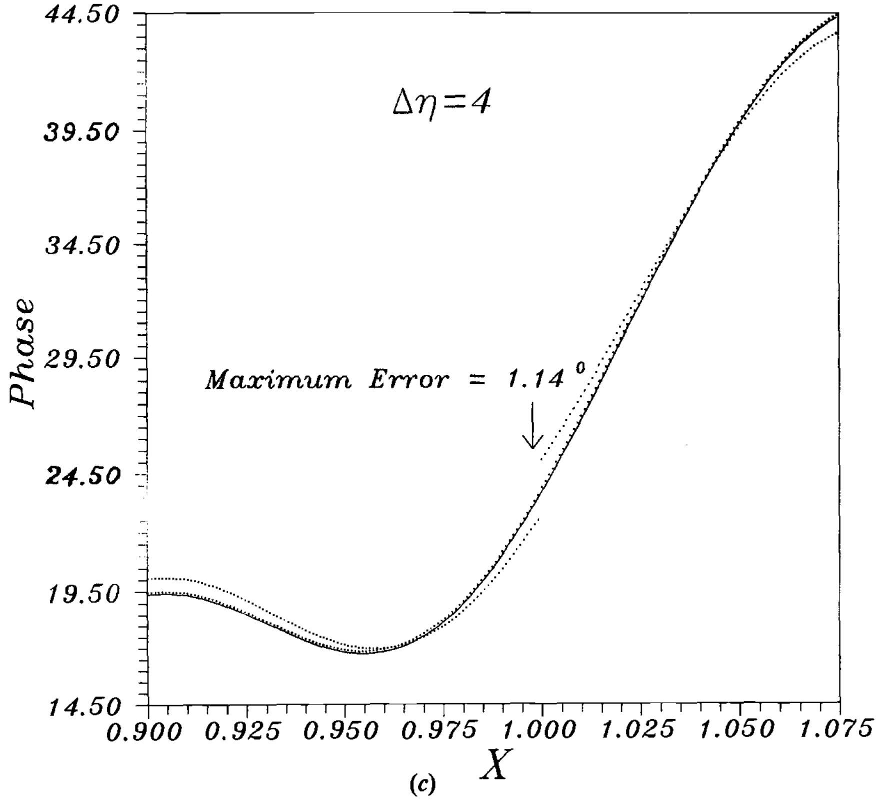

(c)

Figure 9. (*a*) Modulus of the field diffracted by a slit (width = 0, $\Delta\eta = 4$) computed by exact Romberg integration. X is a normalized distance in the diffraction plane. $X = \pm 1$ correspond to the edge of the geometrical shadow. (*b*) Zone of maximum error for the modulus in (*a*) when using exact Romberg integration (continuous line), the GNA procedure (dots close to continuous line), the GAA method (dots further from the line, less accurate). (*c*) As in (*b*), but for the phase.

expression for $k = 0{\cdot}68$. This is the best constant k we have found by testing equation (24) for possible values of k.

In conclusion, when these simple analytical expressions are used to evaluate the previous integrals I_a, $I_b, \ldots$, replacing the numerical techniques (as the Romberg method), the errors induced in modulus and phase are quite small, as represented in figure 8 (*a*) and (*b*).

A special case should be treated with caution: when η lies in the approximate interval 0–3·5. This is because absolute errors now become more significant than relative ones, as in (25) and (26) we use two approximate values to estimate their small difference. Indeed, for this particular case our approximations may be avoided, since this kind of integral is rapidly computed by exact numerical integration, as the integrand does not oscillate rapidly here.

Thus, finally, we propose a geometrically based analytical approximation (GAA) for computing I_∞^η as:

(*a*) for $\eta < 3{\cdot}5$ numerical integration,
(*b*) for $\eta > 3{\cdot}5$ use I_d computed using (17), (20) and (24).

5. Application to the computation of diffraction integrals

We have shown how to simplify the computation of I^{η}_{∞} by means of simpler integrals such as I_1, I_2 and I_4.

Moreover, fairly accurate values may be obtained by simple approximations of these three integrals, using elementary analytical expressions. The remaining problem is to indicate how and when these procedures may be useful for general diffraction integrals where the points limiting the integration interval are unrestricted.

We can distinguish between two cases, depending on the signs of the parameters which represent the initial and final integration points. Equivalently, the cases depend on the quadrants of the position of the points. For a diffraction aperture, the possibilities are.

(*a*) The calculation point lies in the geometrical shadow of the aperture: the limits for the integrals have the same sign. Depending on this sign, the suitable decompositions are

$$\int_{\eta_1}^{\eta_2} \exp(-\mathrm{i}x^2)\,\mathrm{d}x = \int_{\eta_1}^{\pm\infty} \exp(-\mathrm{i}x^2)\,\mathrm{d}x + \int_{\pm\infty}^{\eta_2} \exp(-\mathrm{i}x^2)\,\mathrm{d}x, \qquad (25)$$

leading to two integrals of the previous type.

(*b*) The calculation point lies outside the geometrical shadow: the limits of the integrals have opposite sign and the appropriate decomposition is

$$\int_{\eta_1}^{\eta_2} \exp(-\mathrm{i}x^2)\,\mathrm{d}x = \int_{\eta_1}^{-\infty} \exp(-\mathrm{i}x^2)\,\mathrm{d}x + \int_{-\infty}^{\infty} \exp(-\mathrm{i}x^2)\,\mathrm{d}x + \int_{\infty}^{\eta_2} \exp(-\mathrm{i}x^2)\,\mathrm{d}x, \qquad (26)$$

and the first and last integrals may be computed as before.

As indicated earlier, when $\eta 1$ and $\eta 2$ lie in the approximate interval $-3{\cdot}5$ to $3{\cdot}5$, it is better to carry out direct numerical integrations.

It is important to note that, taking this into account, the final accuracy is always better than 1% and the computation time is always optimum, since exact integrations are used when they are faster and more accurate than approximations. Results are even better when observation distances decrease, i.e. large η (see figures 6 and 8).

6. A particular example

In order to show the effectiveness of our procedures for computing Fresnel diffraction distributions, we have developed a particular example. The geometrical configuration corresponds to a plane illuminated slit of width 2. Figure 9 (*a*) is a plot of the modulus of the diffracted field (for $\Delta\eta = 4$) computed by exact Romberg integration. Figure 9 (*b*) is an enlarged portion of (a) showing the zone of maximum error when using (i) numerical (Romberg) integration, (ii) the GNA and (iii) the

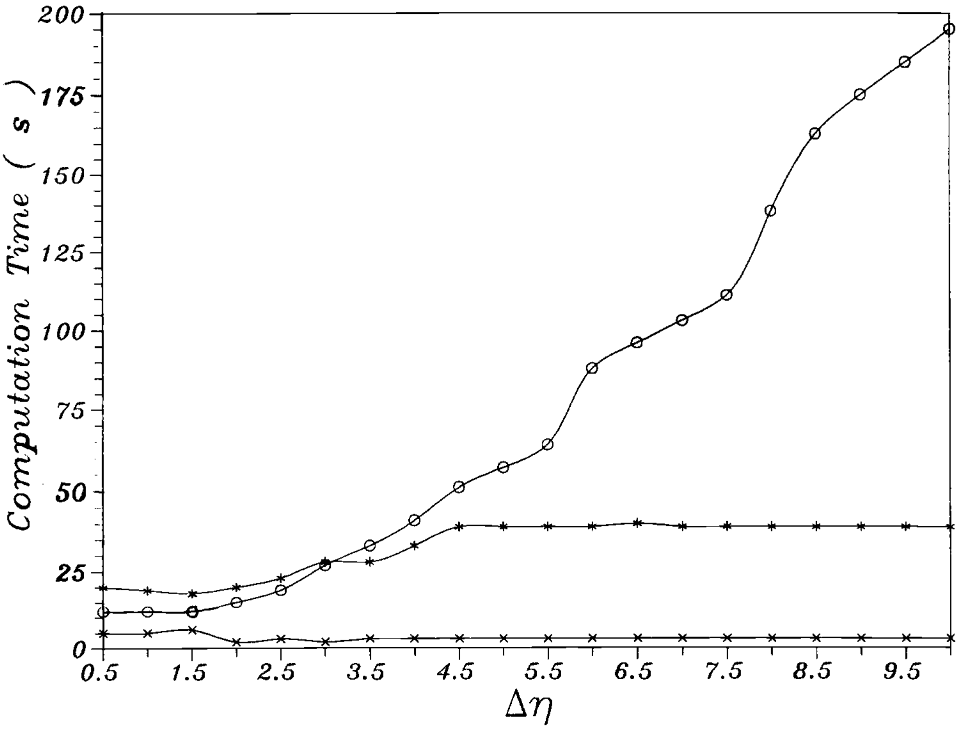

Figure 10. Computation time versus $\Delta\eta$ for a complete one-dimensional Fresnel distribution (modulus and phase). (○) exact Romberg integration (to a fractional accuracy of 10^{-6}), (*) using the GNA procedure, (×) using the GAA method (no numerical integration).

GAA. Figure 9 (*c*) shows the results for the phase. Note that the less accurate zone corresponds to the projection of the edge of the slip, and the least accurate method is GAA. Of course, precision will depend on $\Delta\eta$ (see Section 5).

Figure 10 illustrates the computation times involved when using the three procedures explained, for several values of $\Delta\eta$. The time taken by the GAA is about 3s except in the interval $\Delta\eta < 2$, in which the time is about 5 s. Note that in this case some points are calculated by the exact numerical integration method. For the GNA, the time is about 35 s and it decreases for $\Delta\eta < 3{\cdot}5$. Finally, when exact numerical Romberg integration is used the calculation time increases rapidly with $\Delta\eta$. So, the GAA is the fastest (the time consumed is constant independently of $\Delta\eta$) and the errors are less than 1%.

7. Conclusions

We have developed procedures for the fast and accurate numerical computation of Fresnel diffraction integrals. They are based on geometrical properties inherent to the Cornu spiral, i.e. the length along the curve, the curvature radius and slope of the curve as functions of a single parameter η. Particularly, a central point in our developments is to take a constant curvature radius for small intervals, due to its slow variation as η increases.

Such simple considerations give excellent results in the calculation of modulus and phase of the Fresnel integrals, even when one of the limits of integration falls in the zone of small η values of the spiral. Our methods allow the highly oscillatory integrals in Fresnel diffraction to be approximated by means of three simpler integrals, faster to evaluate. Moreover, geometrically based analytical expressions for these final integrals are also given. This permits a very rapid computation with a moderate loss in accuracy.

Acknowledgments

This work has been supported in part by CICYT project ROB91-0554. E.C. acknowledges the grant given by the Vicerectorat de Recerca de la Universitat de Barcelona.

References

[1] Frieden, B. R., (editor), 1980, *The computer in optical research* (Berlin: Springer-Verlag).
[2] Southwell, W. H., 1981, *J. opt. Soc. Am.*, **71**, 7.
[3] Horwitz, P., 1976, *Appl. Optics*, **15**, 167.
[4] Neff, J. A., Athale, R. A., and Lee, S. H., 1990, *Proc. I.E.E.E.*, **78**, 826.
[5] Klein, M. V., and Furtak, T. E., 1986, *Optics* (New York: John Wiley).
[6] Rossi, B., 1956, *Optics* (Reading, Mass.: Addison-Wesley).
[7] Bruhat, G., 1965, *Cours de Physique générale à l'usage de l'Enseignement Superieur Scientifique et Tecnique: Optique* (Paris: Masson).
[8] Press, W. H., Flannery, B. P., Teukolsky, S. A., and Vetterling, W. T., 1990, *Numerical Recipes in C* (Cambridge University Press), chap. 4.